$\mathcal{PT}$-symmetric direct electrical transmission lines: Localization behavior

Fernando R. Humire* and Edmundo Lazo
Departamento de Física, Facultad de Ciencias, Universidad de Tarapacá, Casilla 7-D Arica, Chile

(Received 4 June 2019; published 26 August 2019)

In this paper, we study a finite direct electrical transmission line when we distribute resistors R_n according to a parity-time ($\mathcal{PT}$) distribution composed of a gain ($-R$) and loss ($+R$) sequence. Considering zero boundary conditions, we find analytical results for the frequency spectrum $\omega(R, k_d)$ as a function of resistance R and the wave number k_d. A frequency spectrum analysis shows a phase transition from real to complex eigenvalues as a function R for fixed $k_{d=N}$, where $2N$ is the size of the transmission line. Numerically, we study localization properties through the normalized localization length $\Lambda(R, k_d)$. This measure shows good agreement with the analytical results and gives an account of the $\mathcal{PT}$-phase transition. Our results pave a solid way toward studying the interplay between parity-time symmetry concepts and one-dimensional electrical transmission lines, aiming to find another generation of electronic devices capable of controlling the flow of energy.

DOI: 10.1103/PhysRevE.100.022221

I. INTRODUCTION

In the last decades, parity-time ($\mathcal{PT}$-) symmetric systems have been the subject of intense research in many areas of physics. These systems were introduced for the first time by Bender and Boettcher [1] in the context of non-Hermitian quantum mechanics. Basically, the authors studied a set of non-Hermitian Hamiltonians that satisfy joint transformations of spatial reflection $\mathcal{P} : x \to -x$ and time reversal $\mathcal{T}$, given by complex conjugation. These non-Hermitian Hamiltonians have a parameter region with a completely real spectrum (unbroken $\mathcal{PT}$-symmetric phase) and a region with a conjugated complex spectrum (broken $\mathcal{PT}$-symmetric phase). The transition point between the unbroken and broken $\mathcal{PT}$-symmetric phase is known as the exceptional point [2].

Behind the concept of $\mathcal{PT}$ symmetry is the condition that the loss and gain in a system are exactly balanced and thus result in bounded dynamics [3]. With this approach, the concept was quickly extended to other disciplines of physics such as optical [4–6], mechanical [7–9], and electronic systems [10,11], among others [2]. Experimentally, optical and electronic classical systems have been shown to be flexible to observe the spontaneous $\mathcal{PT}$-symmetry rupture [10–13].

In the context of finite one-dimensional structures, the effects of different gain and loss configurations have been studied, which include the tight-binding model [14–16], optic models [5,17,18], and artificial electromagnetic materials [3,19]. A widely used configuration consists of an alternating distribution of gain-loss elements, also known as stacks of periodic $\mathcal{PT}$-symmetric structures [19–22]. This configuration presents interesting applications in optical switching devices [20] and nonreciprocal wave propagation [21]. Another kind of configuration has been studied in Ref. [23], where the authors use a one-dimensional photonic quasicrystal in the context of $\mathcal{PT}$ symmetry. Their study focuses on structure properties, which support topological edge modes in their band gaps induced by the $\mathcal{PT}$-symmetric configuration. In general, for parity-time-symmetric finite lattices, it has been shown that the symmetry is conserved within a window of parameters whose size is reduced when the number of sites increases [3,18,24]. Hence, based on the concept of $\mathcal{PT}$ symmetry, the development of new artificial materials and structures has been one of the main topics of research in many areas of physics. It has also been shown, theoretically and experimentally, that these media with balanced loss and gain can exhibit several intriguing characteristics that at present are unobtainable with standard arrangements [25]. For example, in optics, they include phenomena of unidirectional propagation and the nonreciprocal wave propagation [12,26].

On the other hand, a system recently studied is the ideal discrete electrical transmission line (TL). Interest in this classic electrical system is addressed in studies of localization properties considering periodic, aperiodic, quasiperiodic, and long-range correlated distribution of capacitances and inductances [27–34]. The localization properties were also studied for disordered linear and nonlinear electrical lattices [35–40]. However, these systems are incompatible with dissipative elements, i.e., electrical resistances, because any resistance value will render the conduction properties unstable and a greater injection of energy will be necessary to compensate for the dissipation. In this line, $\mathcal{PT}$-symmetric electrical TL models have been proposed in magnetic metamaterials [3] and in noninvasive techniques to detect glucose changes [41].

In this paper, we work on a one-dimensional finite electrical transmission line in its direct configuration. We introduce a distribution of electric resistances R_n, which is alternately distributed as gain ($-R$) and loss ($+R$) on the horizontal elements of TL. Using zero boundary conditions and owing to the fact that the distribution of resistances is horizontal, we can derive analytical expressions for characteristic frequencies $\omega(k_d, R)$ that govern the dispersion properties of the one-dimensional electrical TL. For a completely real spectrum, i.e., when the gain-loss parameter R is less than a critical value R_c,

*f.humire@academicos.uta.cl

we show that the presence of the $\mathcal{PT}$-symmetric resistance distribution favors the conduction properties of the electric current function. By increasing the gain-loss parameter R, we find a region where the current function is attenuated to zero. The transition from the extended to dissipative state, and control of it, is impossible in ideal TLs. In addition, we find an expression for the critical point $R_c(N, Z_0)$ as a function of the system size N and the characteristic impedance Z_0. For fixed N, the unbroken $\mathcal{PT}$ phase grows when the characteristic impedance Z_0 increases. For increasing system size N, R_c goes to zero.

We are also interested in studying the localization properties of the $\mathcal{PT}$-symmetric TL. To do that, we use the normalized localization length $\Lambda(R, \omega)$ and the electric current function $I_n(R, \omega)$ as a function of the frequency ω and the gain-loss parameter R. $\Lambda(R, \omega)$ can accurately find the critical resistance R_c, which separates the different phases of the $\mathcal{PT}$-symmetric problems.

This paper is organized as follows. In Sec. II, we introduce the $\mathcal{PT}$-symmetric direct electric transmission line model. Next, we propose a plane-wave-type solution to obtain an analytical expression of eigenfrequencies that govern the evolution of the system. In Sec. III, we show results and provide discussions. Last, conclusions and final remarks appear in Sec. IV.

II. THE MODEL

In this section, we introduce the $\mathcal{PT}$-symmetric direct electrical transmission line which is formed by a horizontal distribution of inductances L_n, a vertical distribution of capacitances C_n, and a horizontal distribution of resistances R_n according to a gain-loss sequence. The latter is defined as

$$R_n = \begin{cases} +R, & n \text{ even}, \\ -R, & n \text{ odd}, \end{cases} \tag{1}$$

where $n = 0, \ldots, (2N + 1)$ and $+R$ and $-R$ account for dissipative (loss) and active (gain) elements of the system, respectively. Notice that our paper describes a theoretical model, which simultaneously considers gain $(-R)$ and loss $(+R)$ in the direct transmission line. The practical implementation of the negative resistance (using nonlinear devices) has been recently proposed in two different ways: (a) using operational amplifier devices [10,41] and (b) using photocells connected to a metal-oxide semiconductor field-effect transistor (MOSFET) [42].

Figure 1 shows the $\mathcal{PT}$-symmetric direct TL configuration. Applying the Kirchhoff loop rule to three successive unit cells of our $\mathcal{PT}$-symmetric direct TL model allows us to obtain a dynamic equation relating the electric current $i_n(t)$ circulating in $(n-1)$th, nth, and $(n+1)$th cells. Thus we get

$$L_n \frac{d^2 i_n}{dt^2} + R_n \frac{di_n}{dt} + \frac{1}{C_n}(i_n - i_{n+1}) + \frac{1}{C_{n-1}}(i_n - i_{n-1}) = 0. \tag{2}$$

Here, we consider zero boundary conditions at cells $n = 0$ and $n = (2N + 1)$. Also, the capacitances and inductances in each cell are considered constants, i.e., $L_n = L$ and $C_n = C\ \forall n$. The equations of motion (2) are reduced to

$$\frac{di_n}{dt} = p_n, \tag{3a}$$

$$\frac{dp_n}{dt} = -\beta_n p_n + \omega_0^2 (i_{n-1} - 2i_n + i_{n+1}), \tag{3b}$$

where $\beta_n = R_n/L$ is the damping coefficient and $\omega_0 = \sqrt{1/(LC)}$ is the natural frequency of each cell. This system of equations is $\mathcal{PT}$ symmetric under the following transformations [43],

$$\mathcal{P} : i_n \to -i_{2N-n+1}, \quad p_n \to -p_{2N-n+1}, \tag{4a}$$

$$\mathcal{T} : i_n \to i_n, \quad p_n \to -p_n, \tag{4b}$$

where $1 \leqslant n \leqslant 2N$. Next, for the electric current intensity $i_n(t)$, we use zero boundary conditions at cells $n = 0$ and $n = (2N + 1)$, and using the Fourier transform on each site, we obtain

$$\left[2 - \left(\frac{\omega}{\omega_0}\right)^2 + i\beta_n \frac{\omega}{\omega_0^2}\right] I_n - I_{n-1} - I_{n+1} = 0, \tag{5}$$

where $I_n(\omega)$ is the complex amplitude of the electric current intensity at site n, and ω is the vibration frequency of each site. Based in classical and quantum solutions used in $\mathcal{PT}$-symmetric problems [7,15,44], we propose solutions of Eq. (5) in the form

$$I_n = \begin{cases} A\cos(nk) + B\sin(nk), & n \text{ even}, \\ \epsilon[A\cos(nk) + B\sin(nk)], & n \text{ odd}. \end{cases} \tag{6}$$

Applying the zero boundary conditions $I_0 = 0$ and $I_{(2N+1)} = 0$ on the previous solution, we obtain discrete values for k as

$$k_d = \left(\frac{\pi}{2N+1}\right) d, \tag{7}$$

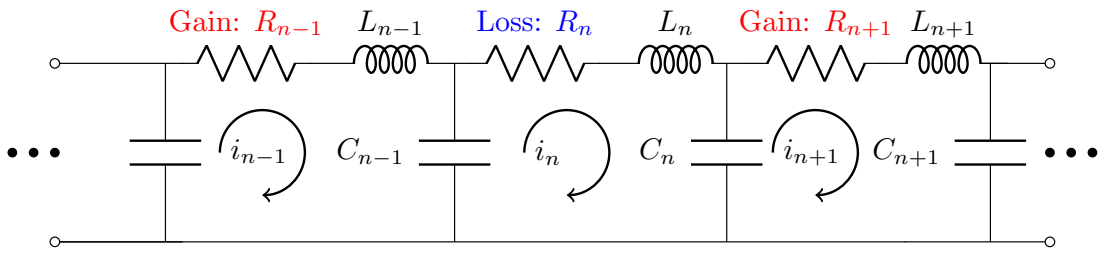

FIG. 1. A $\mathcal{PT}$-symmetric resistance configuration in a direct electrical transmission line.

where $d = 1, \ldots, N$. Replacing the solution (6) into Eq. (5) and considering the $\mathcal{PT}$-symmetric resistive configuration R_n (1), it turns out that

$$\left[2 - \left(\frac{\omega}{\omega_0}\right)^2 + i\beta\frac{\omega}{\omega_0^2}\right] = 2\epsilon\cos(k), \quad n \text{ even}, \tag{8a}$$

$$\epsilon\left[2 - \left(\frac{\omega}{\omega_0}\right)^2 - i\beta\frac{\omega}{\omega_0^2}\right] = 2\cos(k), \quad n \text{ odd}, \tag{8b}$$

where $\beta = R/L$. Next, combining these equations and remembering the discrete relation (7), we obtain the equation for the frequency spectrum $\omega(R, k_d)$,

$$\omega^4 + 4\omega_0^2 M\omega^2 + 4\omega_0^4 \sin^2(k_d) = 0, \tag{9}$$

where $M = (\frac{\beta}{2\omega_0})^2 - 1$. Solutions are given by

$$\omega^2(R, k_d) = 2\omega_0^2[-M \pm \sqrt{M^2 - \sin^2(k_d)}], \tag{10}$$

The unbroken $\mathcal{PT}$-symmetric phase only exists for real frequencies, and this condition is fulfilled by the following relations,

$$\text{(I) } M^2 - \sin^2(k_d) \geqslant 0, \quad \text{(II) } M > 0. \tag{11}$$

In addition, we impose the condition that the real part of the $\omega(R, k_d)$ frequencies is always positive; we denote them as $\omega_{1,2}(R, k_d)$.

From (11) we obtain two conditions for R as a function of k_d, namely,

$$R \leqslant R_{\pm}(k_d) = 2Z_0\sqrt{1 \pm \sin(k_d)}, \tag{12}$$

where $Z_0 = \sqrt{L/C}$ is the characteristic impedance of ideal TL and $d = 1, \ldots, N$. We note that when condition $R \leqslant R_-(k_d)$ is fulfilled, the other condition $R \leqslant R_+(k_d)$ is also fulfilled for any wave number k_d. Then, for each value of $d < N$, the spectrum is constituted by complex and real eigenvalues. However, for $d = N$ the spectrum only contains real eigenfrequencies since the function $R_-(k_d)$ takes its smallest value. For this value, $d = N$, the phase transition occurs for the critical resistance R_c, i.e.,

$$R_c = R_-(k_{d=N}) = 2Z_0\sqrt{1 - \sin(k_N)}, \tag{13}$$

where $k_{d=N} = \pi N/(2N + 1)$. Conversely, for $d = 1$ we obtain the greatest value of the function $R_-(k_d)$, and as a consequence, for $R > R_{\text{smt}}$ we obtain a spectrum completely complex without real eigenvalues, where

$$R_{\text{smt}} = R_-(k_{d=1}) = 2Z_0\sqrt{1 - \sin(k_1)}, \tag{14}$$

with $k_{d=1} = \pi/(2N + 1)$ [see Fig. 3(a)]. Finally, the function $R_+(k_d)$ takes its greatest value for $d = N$ and its spectrum only contains imaginary eigenvalues, that is,

$$R_I = R_+(k_{d=N}) = 2Z_0\sqrt{1 + \sin(k_N)}. \tag{15}$$

Next, using expression (8) and the zero boundary conditions, we can find the $I_n(k_d)$ electric current (6) as

$$I_n(k_d) = \begin{cases} 2iA\sin(nk_d), & n \text{ even}, \\ 2iA\epsilon_d\sin(nk_d), & n \text{ odd}, \end{cases} \tag{16}$$

where $\epsilon_d = e^{i\delta_d}$ and A is a constant that can be determined by the normalization condition. δ_d is defined as

$$\tan\delta_d = \frac{\tau\omega_{1,2}(R, k_d)}{2 + \left(\frac{\omega_{1,2}(R,k_d)}{\omega_0}\right)^2}. \tag{17}$$

If $\omega_{1,2}(k_d, R)$ are real, we obtain the following amplitudes,

$$|I_n(k_d)| = \begin{cases} 2|A|\sin(nk_d), & n \text{ even}, \\ 2|A|\sin(nk_d), & n \text{ odd}, \end{cases} \tag{18}$$

where

$$|A|^2 = \frac{1}{4N - 2\frac{\sin(2Nk_d)}{\sin(k_d)}(-1)^d}. \tag{19}$$

Otherwise, if $\omega_{1,2}(k_d, R)$ are complex numbers, δ_d is also a complex number. Thus, the current intensity is given by

$$|I_n(k_d)| = \begin{cases} 2|A|\sin(nk_d), & n \text{ even}, \\ 2|A||\epsilon_d|\sin(nk_d), & n \text{ odd}, \end{cases} \tag{20}$$

where

$$|A|^2 = \frac{1}{4}\left(\sum_{n=1}^{N} p_n(\epsilon_d)\right)^{-1}, \tag{21}$$

with

$$p_n(\epsilon_d) = \sin^2(2Nk_d) + |\epsilon_d|^2\sin^2[(2n - 1)k_d]. \tag{22}$$

III. RESULTS AND DISCUSSION

In this section, we analyze the transition from a completely real spectrum (unbroken $\mathcal{PT}$-symmetry phase) characterized by extended current functions to a complex spectrum (broken $\mathcal{PT}$-symmetry phase) characterized by dissipative current functions. In all figures, we use the following parameter values: $N = 30$ [except for Fig. 3(b)], $L = 1(\mu\text{H})$, and $C = 10(\text{nF})$.

In Fig. 2 the real $\text{Re}(\omega)$ and imaginary $\text{Im}(\omega)$ parts of eigenvalues $\omega_{1,2}(R, k_d)$ appear as a function of wave number k_d, considering several values of the gain-loss parameter $R = \{0.2, 5, 16, 30\}(\Omega)$. For $R = 0.2(\Omega) < R_c$ where $R_c(k_{d=30}) = 0.3642(\Omega)$, Figs. 2(a) and 2(b) show the frequency range where the unbroken $\mathcal{PT}$-symmetric region exists, since the imaginary part $\text{Im}(\omega_{1,2})$ is equal to zero. For R values such as $R_c < R = \{5, 16\} < R_{\text{smt}} = 19.48(\Omega)$, Figs. 2(c) and 2(d) show that eigenfrequencies begin to leave the unbroken $\mathcal{PT}$ phase, since the condition (12) is not fulfilled for all wave numbers k_d. When R grows, $R \to R_{\text{smt}}$, the transition point P moves to $k_{d=1}$. This point P separates the region with real eigenvalues $\omega(k_d, R) = \omega_R(k_d, R)$ from the region with complex eigenvalues $\omega(k_d, R) = \omega_R(k_d, R) + i\omega_I(k_d, R)$. For $R = 30(\Omega) > R_I = 28.28(\Omega)$, eigenvalues in Figs. 2(e) and 2(f) are of the form $\omega(k_d) = i\omega_I(k_d, R)$ (the broken $\mathcal{PT}$-symmetric region).

Figure 3(a) shows $R_{\pm}(k_d)$ as a function of k_d. The red-asterisk dashed line is R_+ and the blue-circle solid line is R_-. Here, we observe that if the condition (12) is satisfied for all k_d, we can find the critical resistance R_c as $R_c = 2Z_0\sqrt{1 - \sin(k_N)} = 0.3642(\Omega)$. The unbroken $\mathcal{PT}$-symmetric phase occurs for $R \leqslant R_c$, getting a completely real spectrum. Also, Fig. 3(a) shows four regions: (i) For

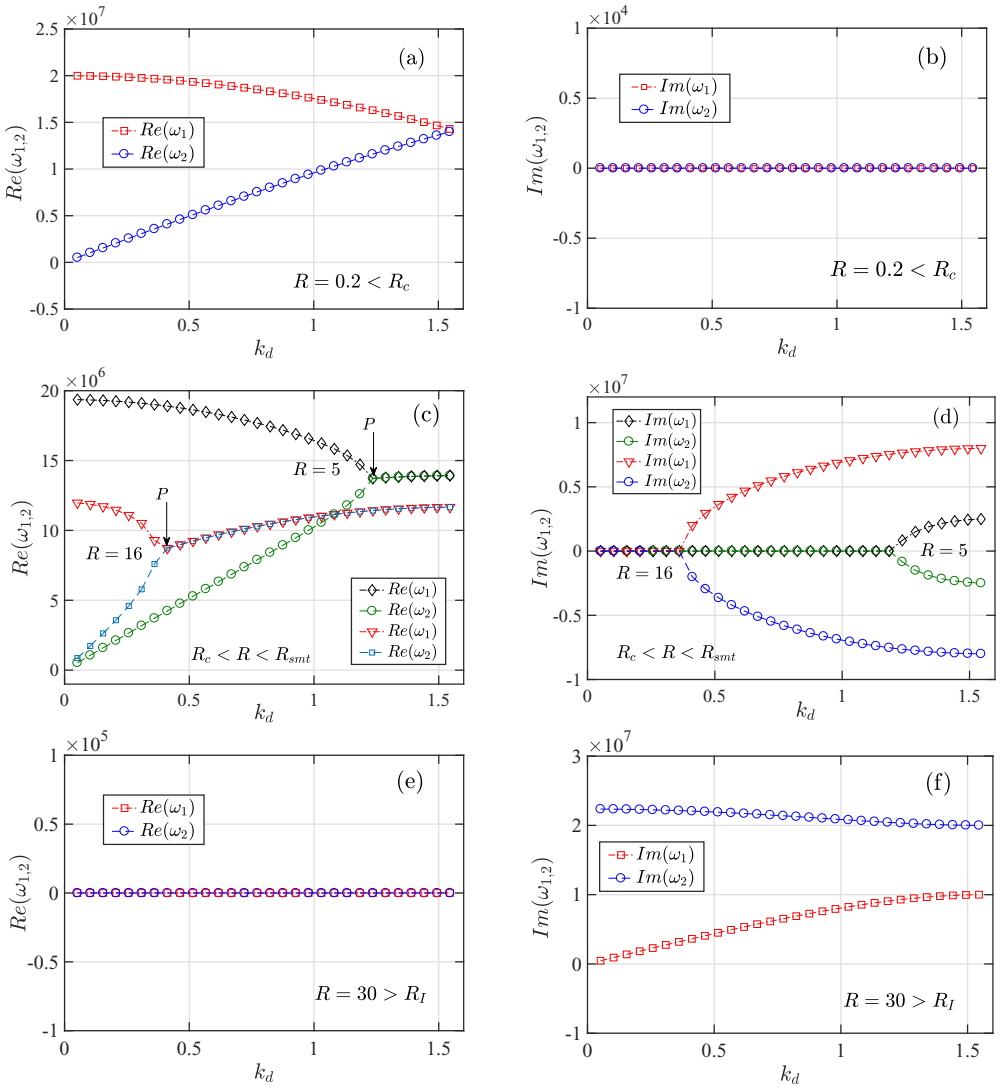

FIG. 2. A sequence of the real and imaginary part of $\omega_{1,2}(k_d, R)$ as a function of k_d for several values of the gain-loss parameter R for $N = 30$. (a), (b) Completely real spectrum for $R = 0.2(\Omega) < R_c$ and (c), (d) both real and imaginary eigenvalues for $R = \{5, 10, 16\}(\Omega)$ with $R > R_c$. (e), (f) Completely imaginary spectrum for $R = 30(\Omega)$.

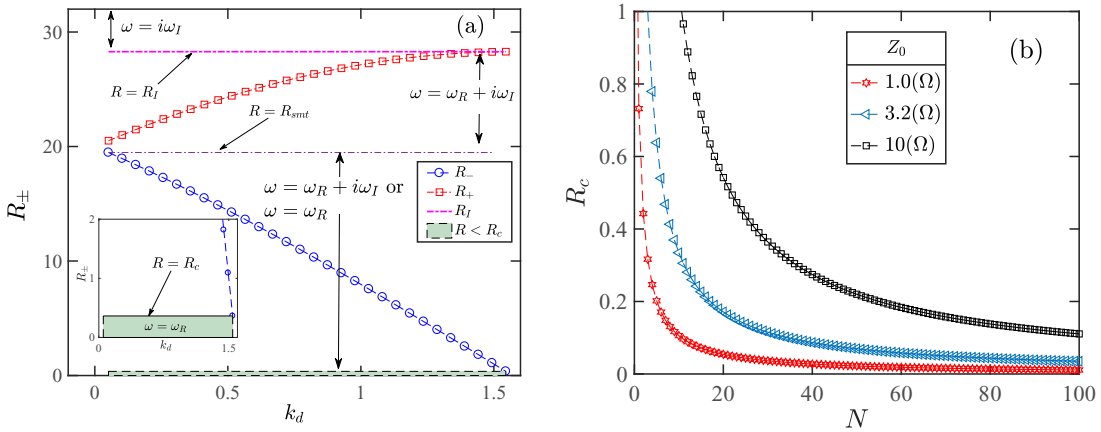

FIG. 3. (a) Resistance function $R_\pm$ as a function of k_d with $N = 30$, $R = R_c(k_{N=30}) = 0.3642(\Omega)$ (black dashed line), and $R_I = 28.28(\Omega)$ (pink dashed-dotted line). The inset shows a zoom of the unbroken $\mathcal{PT}$-symmetric region; the condition of a completely real spectrum is defined in Eq. (12) with $d = N$. (b) Critical resistance R_c as a function of N for different values of characteristic impedance $Z_0 = 1.0(\Omega)$, $Z_0 = 3.2(\Omega)$, and $Z_0 = 10(\Omega)$.

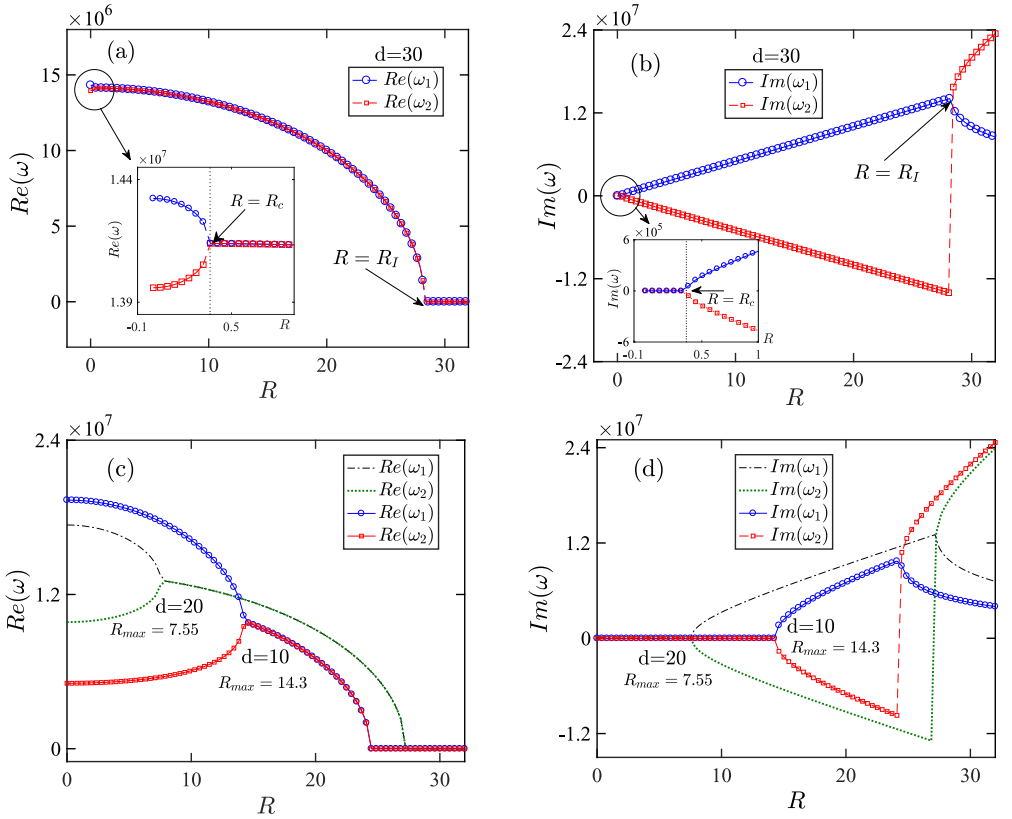

FIG. 4. Real Re(ω) and imaginary Im(ω) part of the frequency spectrum $\omega_{1,2}(R, k_d)$ as a function of R for different values of the parameter $d = \{30, 20, 10\}$. (a), (b) $d = N = 30$, in both panels, the insets show a zoom of the unbroken $\mathcal{PT}$-symmetric region. (c), (d) $d = \{20, 10\}$ with $d < N$. For $d = 20$, $R_{\max} = R_{-}(k_{d=20}) = 7.55(\Omega)$ and for $d = 10$, $R_{\max} = R_{-}(k_{d=10}) = 14.3(\Omega)$.

$R < R_c$, eigenvalues are real $\omega = \omega_R$ (green shaded region), (ii) for $R_c < R < R_{\rm smt} = R_{-}(k_{d=1}) = 19.48(\Omega)$, eigenvalues can be real $\omega = \omega_R$ or complex numbers $\omega = \omega_R \pm i\omega_I$, (iii) for $R_{\rm smt} < R < R_I$, eigenvalues are complex numbers $\omega = \omega_R \pm i\omega_I$, and (iv) for $R > R_I$, eigenvalues are imaginary numbers $\omega = \pm i\omega_I$. The figure inset clearly shows the green shaded region with a real frequency spectrum $\omega = \omega_R$ and critical resistance $R_c = 0.3642(\Omega)$. Therefore, the unbroken $\mathcal{PT}$-symmetric phase is only valid for $R \leqslant R_c(k_N)$ and the broken $\mathcal{PT}$-symmetric phase is valid for $R > R_c(k_N)$.

Figure 3(b) displays the critical resistance $R_c(k_N)$ as a function of N for three values of characteristic impedance, namely, $Z_0 = 1.0(\Omega)$ (red-star dashed line), $3.2(\Omega)$ (blue-star dashed line), and $10(\Omega)$ (black-square dashed line). We observe that when $N \gg 1$, $k_d \to \pi/2$, and the critical resistance goes to zero ($R_c \to 0$), independently of the value of Z_0, which indicates that the unbroken $\mathcal{PT}$ phase disappears and as a consequence the real eigenvalues are absent. Conversely, for N small and for increasing values of characteristic impedance Z_0, the critical resistance R_c increases and the amplitude of the unbroken $\mathcal{PT}$-symmetric region also increases.

Figure 4 shows the frequency spectrum $\omega(R)$ as a function of gain-loss parameter R. Figures 4(a) and 4(c) show the real part Re(ω), and Figs. 4(b) and 4(d) show the imaginary part Im(ω). In the panels above with $d = N = 30$, we can observe that for $R \geqslant R_I$ all eigenvalues are imaginary $\omega = i\omega_I$. The insets show the unbroken $\mathcal{PT}$ phase [$R \leqslant R_c$, see Eq. (13)] and the critical point at $R_c = R_{-}(k_{d=N})$. In the panels below with $d = \{10, 20\}$, we show the points $R_{\max} = R_{-}(k_{d=20}) = 7.55(\Omega)$, $R_{\max} = R_{-}(k_{d=10}) = 14.3(\Omega)$, and their corresponding conducting regions $R \leqslant R_{\max} = 7.55(\Omega)$ and $R \leqslant R_{\max} = 14.3(\Omega)$. Even though the spectrum has real and complex eigenvalues (broken $\mathcal{PT}$ phase), we can get a conducting region larger than in the case $d = N$. In this region, the electric current has extended behavior. This is due exclusively to the $\mathcal{PT}$-symmetric resistance configuration.

Typical electric current functions are shown in Fig. 5(a). For $R = 0.23(\Omega) < R_c$, we observe that $|I_n|$ is a symmetrical and extended function for real frequencies $\omega_1 = 1.43 \times 10^7$ and $\omega_2 = 1.40 \times 10^7$ (unbroken $\mathcal{PT}$ phase). In Fig. 5(b), for $R = 31(\Omega) > R_c$, we observe that $|I_n|$ is an asymmetrical and dissipative function for imaginary eigenvalues $\omega_1 = i9.15 \times 10^6$ and $\omega_2 = i2.18 \times 10^7$ (broken $\mathcal{PT}$ phase).

Next, we study localization properties through the normalized localization length $\Lambda(R, \omega)$ which exhibit a clear transition from the resistance R and the frequency ω. We compare the analytical results of Sec. II with the localization criteria for $\Lambda(R, \omega)$, namely, the electric current function is a localized function for $\Lambda(R, \omega) < 1$ and is an extended function for $\Lambda(R, \omega) \geqslant 1$. The $\xi(R, \omega)$ localization length is defined as

$$\xi^{-1}(R, \omega) = \lim_{M \to \infty} \frac{1}{M} \sum_{n=1}^{M} \ln \left| \frac{I_{n+1}}{I_n} \right|, \tag{23}$$

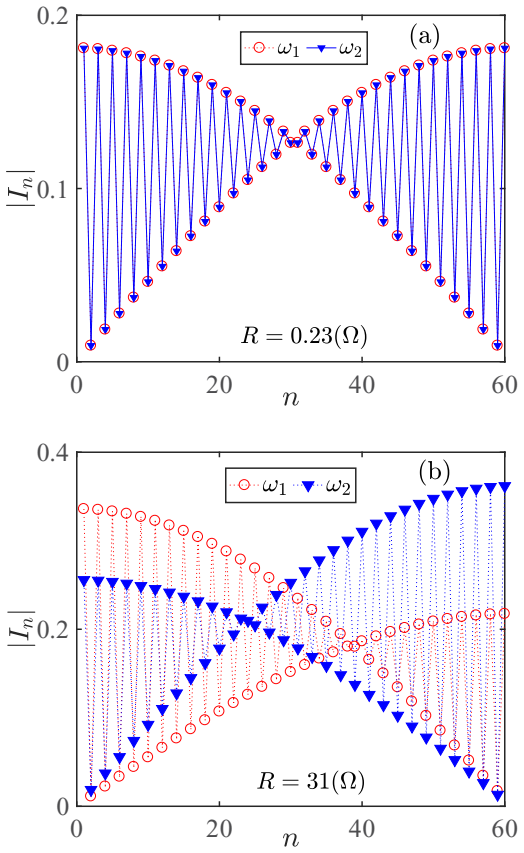

FIG. 5. Modulus of the electric current function $|I_n|$ as a function of n for both frequencies $\omega_{1,2}(R, k_d)$. (a) Symmetric and extended state for $R = 0.23(\Omega) < R_c$ with frequencies $\omega_1 = 1.43 \times 10^7$ (rad/s) and $\omega_2 = 1.40 \times 10^7$ (rad/s). (b) Asymmetrical and dissipative state for $R = 31(\Omega) > R_I$ with eigenvalues $\omega_1 = i9.15 \times 10^6$ (rad/s) and $\omega_2 = i2.18 \times 10^7$ (rad/s).

where $I_n(R, \omega)$ is the amplitude of the electric current function in each nth cell of the TL and M is the size of the system under study. To calculate $\xi(R, \omega)$ we solve Eqs. (5) through an iterative process that deploys the transfer function Γ_n defined as

$$\Gamma_n(R, \omega) = \frac{I_{n+1}}{I_n}. \tag{24}$$

Using (24), Eqs. (5) can be written in the following iterative way,

$$\Gamma_n = \left[2 - \left(\frac{\omega}{\omega_0}\right)^2 + i\omega R_n C\right] - (\Gamma_{n-1})^{-1}. \tag{25}$$

Starting with $\Gamma_1 = [2 - (\frac{\omega}{\omega_0})^2 + i\omega R_1 C]$, we can get all the Γ_n transfer functions and, after that, we can calculate $\xi(R, \omega)$ in the following form,

$$\xi^{-1}(R, \omega) = \lim_{M\to\infty} \frac{1}{M} \sum_{n=1}^{M} \ln |\Gamma_n(R, \omega)|. \tag{26}$$

The localization behavior of the direct TL is studied using the normalized localization length $\Lambda(R, \omega)$ defined as $\Lambda(R, \omega) = \frac{\xi(R,\omega)}{M}$. Even though we are working with TLs with very few cells ($M = 2N \leqslant 60$), $\Lambda(R, \omega)$ is still able to accurately discriminate between localized states [$\Lambda(R, \omega) < 1$] and extended states [$\Lambda(R, \omega) \geqslant 1$]. We study the localization behavior of the $\mathcal{PT}$-symmetric direct TL calculating $\Lambda(R, \omega)$ as a function of the resistance R and as a function of the frequency ω, in the following two different cases: (a) when the frequencies $\omega_{1,2}$ are known functions of the resistance R [see Eq. (10)], and (b) when the frequency ω and the resistance R are variables completely independent between them.

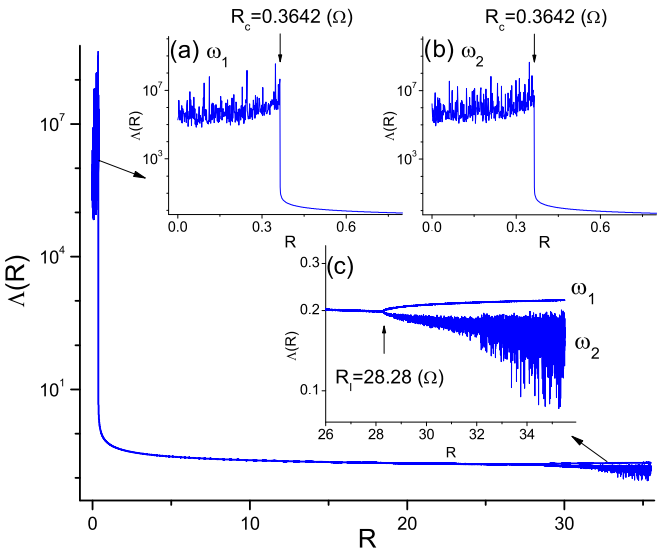

FIG. 6. Case (a): Normalized localization length $\Lambda(R, \omega_1)$ and $\Lambda(R, \omega_2)$ vs R for fixed $N = 30$ and $k_{d=N}$. For both frequencies ω_1 and ω_2, $\Lambda(R, \omega)$ determines three regions with different localization behaviors, which are delimited by critical points $R_c = 0.3642(\Omega)$ and $R_I = 28.28(\Omega)$ (see insets). For $R \leqslant R_c$, insets (a) ω_1 and (b) ω_2 show a zoom of the unbroken $\mathcal{PT}$-symmetric phase which corresponds to extended electric current functions [$\Lambda(R, \omega_{1,2}) \geqslant 1$]. For $R > R_c$ we can only find a dissipative behavior which corresponds to the broken $\mathcal{PT}$-symmetric phase [$\Lambda(R, \omega_{1,2}) < 1$]. Inset (c) shows $\Lambda(R, \omega_{1,2})$ in the neighborhood of $R_I = 28.28(\Omega)$.

A. Case (a)

In this case, for each R value, the critical frequencies $\omega_{1,2}$ are obtained using Eq. (10) and for these specific frequencies we calculate $\Lambda(R, \omega)$. In Fig. 6 we show $\Lambda(R, \omega_1)$ and $\Lambda(R, \omega_2)$ for fixed $N = 30$ and $k_{d=N} = 1.545$, when R varies on a wide range, i.e., $R \in (0, 36(\Omega)]$. In this figure we can see that $\Lambda(R, \omega)$ can distinguish three zones:

(i) $R \in (0, R_c = 0.3642(\Omega)]$. In this first zone we only find extended states [$\Lambda(R, \omega) \geqslant 1$], as can be seen in upper insets (a) and (b) of Fig. 6. Also, these insets show the unbroken $\mathcal{PT}$-symmetric region, where all eigenfrequencies are real. This result also appears in the inset of Fig. 3(a), where we show the critical resistance $R = R_c$.

(ii) $R \in (R_c, R_I = 28.28(\Omega)]$. Here, we only find localized states [$\Lambda(R, \omega) < 1$], which corresponds to the broken $\mathcal{PT}$-symmetric phase, because the frequency spectrum has real and imaginary values.

(iii) $R > R_I$. Here, we only find localized states [$\Lambda(R, \omega) < 1$], which also corresponds to the broken $\mathcal{PT}$-

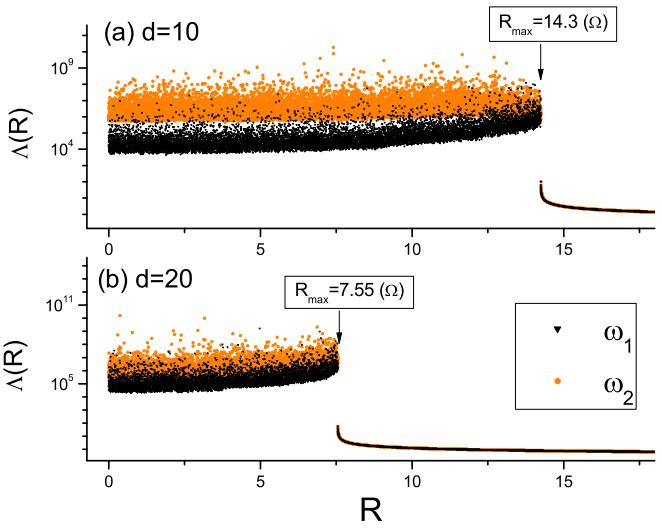

FIG. 7. Case (a): $\Lambda(R,\omega)$ vs R for frequencies ω_1 and ω_2, for the case $d < N = 30$ which corresponds to the broken $\mathcal{PT}$-symmetric phase, where the frequency spectrum has real and complex eigenvalues. For each frequency we find a resistance $R_{\max}$. For $R \leqslant R_{\max}$ we obtain symmetrical extended functions $[\Lambda(R) \geqslant 1]$. (a) For $d = 10$ we obtain $R_{\max} = 14.3(\Omega)$ and (b) for $d = 20$ we obtain $R_{\max} = 7.55(\Omega)$ (see vertical arrows). For $R > R_{\max}$ we obtain asymmetrical localized functions, because $\Lambda(R) < 1$.

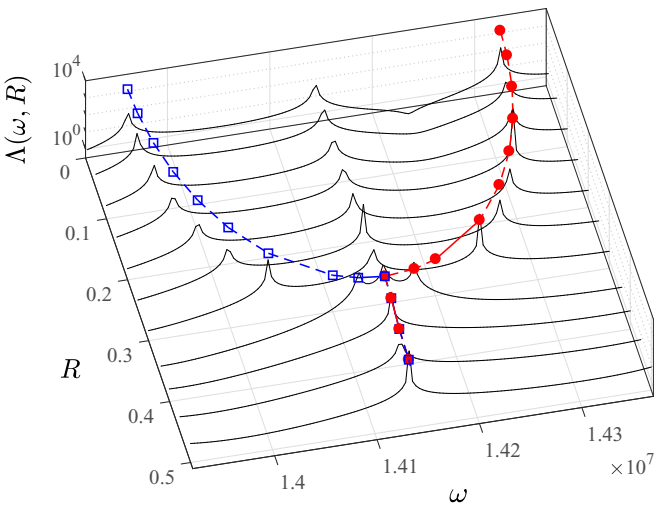

FIG. 8. Case (b): $\Lambda(R,\omega)$ vs ω for each R in the region where the frequencies are real functions. The position of the left and right maxima indicates exactly the frequency values ω_1 and ω_2 with $\Lambda(R,\omega_{1,2}) \geqslant 1$ (extended behavior). The central peak only separates the solutions corresponding to both frequencies. On the top of this figure we superimpose the curves corresponding to $\omega_1(R)$ (open blue square) and $\omega_2(R)$ (solid red circle), for a constant value of $\Lambda_0 > \Lambda_{\max}(R,\omega)$.

symmetric phase, since the frequency spectrum is purely imaginary. The bottom inset (c) of Fig. 6 shows this broken $\mathcal{PT}$-symmetric region. This way we have demonstrated that $\Lambda(R,\omega)$ accurately determines points $R_c = 0.3643(\Omega)$ and $R_I = 28.28(\Omega)$, and the analytic results were illustrated in Fig. 3(a).

Figure 7 shows the $\Lambda(R,\omega)$ normalized localization length versus the resistance R for frequencies ω_1 and ω_2, for the case $d < N = 30$. For $d < N$, the frequency spectrum is formed by real and complex eigenfrequencies, which is an indication that we are inside the broken $\mathcal{PT}$-symmetric phase. Figure 7(a) with $d = 10$ and Fig. 7(b) with $d = 20$ show the existence of a resistance $R_{\max}$. Only for $R \leqslant R_{\max}$ do we obtain symmetrical extended functions, because $\Lambda(R) \geqslant 1$. For $d = 20$ we obtain $R_{\max} = 7.55(\Omega)$ and for $d = 10$ we obtain $R_{\max} = 14.3(\Omega)$ (see vertical arrows). These numerical results describe exactly the same behavior shown in Fig. 4(c). At the same time, this result tells us that $\Lambda(R)$ is an adequate tool to discriminate symmetrical extended functions [real eigenvalues and $\Lambda(R) \geqslant 1$] from asymmetrical localized functions [complex eigenvalues and $\Lambda(R) < 1$].

B. Case (b)

In this case, for fixed $N = 30$, we study $\Lambda(R,\omega)$ as a function of the frequency ω only in the first region of the resistance values, namely, $R \in [0, R_c = 0.3642(\Omega)]$. We do that because we must solve Eq. (5) considering the frequency ω as an independent variable. In Fig. 8 we can see $\Lambda(R,\omega)$ as a function of the ω frequency for each R in the region where the frequencies are real functions, i.e., for $\omega \in [1.38 \times 10^7, 1.45 \times 10^7]$. There we can see three peaks corresponding to the maximum value of $\Lambda(\omega)$ with $\Lambda(R,\omega) > 1$. The central peak separates solutions corresponding to frequency ω_1 from the solutions corresponding to frequency ω_2. The position of the central maximum moves very little when R varies. In addition, the position of the left and right maxima indicates exactly the position of frequencies ω_1 and ω_2, which numerically coincides with the values analytically obtained from Eq. (10). On the top of this figure we superimpose the curves corresponding to $\omega_1(R)$ (open blue square) and $\omega_2(R)$ (solid red circle), for a constant value of $\Lambda_0 > \Lambda_{\max}(R,\omega)$.

The superimposed picture is identical to the figure shown in the inset of Fig. 4(a). This way we have shown that the normalized localization length $\Lambda(R,\omega)$ is able to determine the values of the resistance R and the frequencies $\omega_{1,2}$ in which the unbroken $\mathcal{PT}$-symmetric condition is met.

IV. CONCLUSION

We introduced a discrete electric transmission line with a resistance distribution R_n which follows a gain-loss sequence. We obtained closed-form expressions for the corresponding real and positive frequency spectra $\omega_{1,2} = \omega_{1,2}(R, k_d)$ as a function of the gain-loss parameter R and the wave number k_d. This allows us to characterize the $\mathcal{PT}$-phase transition from a region with a completely real spectrum for $R \leqslant R_c = R_-(k_{d=N})$ (unbroken $\mathcal{PT}$ phase) to a region with a complex spectrum for $R > R_c$ which is formed by real and complex eigenvalues (broken $\mathcal{PT}$ phase). However, for $d < N$ we report extended states for $R \leqslant R_-(k_d)$. Also, we can say that in the unbroken $\mathcal{PT}$ phase, the electric current $|I_n|$ is always a symmetrical function. This symmetrical behavior disappears when the system goes to the broken $\mathcal{PT}$ phase. In addition, we are able to control the amplitude of the unbroken $\mathcal{PT}$-symmetric region (the size of R_c) by changing the impedance

Z_0 for fixed N. Conversely, for fixed Z_0 the unbroken $\mathcal{PT}$ phase tends to disappear when the size N of the system increases.

Numerically, we studied the localization properties using the normalized localization length $\Lambda(R, \omega)$ as a function of the resistance R and the wave number k_d. In case (a), we use R and ω as dependent variables, i.e., $\omega_{1,2} = \omega_{1,2}(R)$, whereas in case (b), we consider ω and R as independent variables. In both cases, in the unbroken $\mathcal{PT}$ region ($R \leqslant R_c$) the modulus of the electric current function $|I_n|$ is an extended function ($\Lambda \geqslant 1$). On the contrary, for $R > R_c$, $|I_n|$ is a localized function ($\Lambda < 1$), a behavior which is characteristic of the broken $\mathcal{PT}$ region.

For all the above, the $\mathcal{PT}$-symmetric electrical TL can be used as a device to generate phase transitions through the control of the gain and loss mechanism. Finally, we think that our results represent a step in the application of parity-time symmetry concepts to another generation of electronic devices.

ACKNOWLEDGMENT

F.R.M.-H. thanks Universidad de Tarapacá for financial support through Project No. 4738-19.

[1] C. M. Bender and S. Boettcher, Phys. Rev. Lett. **80**, 5243 (1998).
[2] V. V. Konotop, J. Yang, and D. A. Zezyulin, Rev. Mod. Phys. **88**, 035002 (2016).
[3] M. I. Molina, Phys. Rev. E **89**, 033201 (2014).
[4] R. El-Ganainy, K. G. Makris, D. N. Christodoulides, and Z. H. Musslimani, Opt. Lett. **32**, 2632 (2007).
[5] K. G. Makris, R. El-Ganainy, D. N. Christodoulides, and Z. H. Musslimani, Phys. Rev. Lett. **100**, 103904 (2008).
[6] Z. H. Musslimani, K. G. Makris, R. El-Ganainy, and D. N. Christodoulides, Phys. Rev. Lett. **100**, 030402 (2008).
[7] S. V. Suchkov, S. V. Dmitriev, B. A. Malomed, and Y. S. Kivshar, Phys. Rev. A **85**, 033825 (2012).
[8] C. M. Bender, M. Gianfreda, S. K. Özdemir, B. Peng, and L. Yang, Phys. Rev. A **88**, 062111 (2013).
[9] C. M. Bender, B. K. Berntson, D. Parker, and E. Samuel, Am. J. Phys. **81**, 173 (2013).
[10] J. Schindler, A. Li, M. C. Zheng, F. M. Ellis, and T. Kottos, Phys. Rev. A **84**, 040101(R) (2011).
[11] Y. Choi, C. Hahn, J. W. Yoon, and S. H. Song, Nat. Commun. **9**, 2182 (2018).
[12] C. E. Rüter, K. G. Makris, R. El-Ganainy, D. N. Christodoulides, M. Segev, and D. Kip, Nat. Phys. **6**, 192 (2010).
[13] A. Guo, G. J. Salamo, D. Duchesne, R. Morandotti, M. Volatier-Ravat, V. Aimez, G. A. Siviloglou, and D. N. Christodoulides, Phys. Rev. Lett. **103**, 093902 (2009).
[14] O. Bendix, R. Fleischmann, T. Kottos, and B. Shapiro, Phys. Rev. Lett. **103**, 030402 (2009).
[15] O. Vázquez-Candanedo, J. C. Hernández-Herrejón, F. M. Izrailev, and D. N. Christodoulides, Phys. Rev. A **89**, 013832 (2014).
[16] Y. N. Joglekar, D. Scott, M. Babbey, and A. Saxena, Phys. Rev. A **82**, 030103(R) (2010).
[17] C. Mejía-Cortés and M. I. Molina, Phys. Rev. A **91**, 033815 (2015).
[18] I. V. Barashenkov, L. Baker, and N. V. Alexeeva, Phys. Rev. A **87**, 033819 (2013).
[19] O. V. Shramkova and G. P. Tsironis, Phys. Rev. B **94**, 035141 (2016).
[20] A. Lupu, H. Benisty, and A. Degiron, Photonics Nanostruct. Fundam. Appl. **12**, 305 (2014).
[21] O. V. Shramkova and G. P. Tsironis, in *2015 17th International Conference on Transparent Optical Networks (ICTON)* (IEEE, New York, 2015).
[22] O. V. Shramkova and G. P. Tsironis, IEEE J. Sel. Top. Quantum Electron. **22**, 5000307 (2016).
[23] N. X. A. Rivolta, H. Benisty, and B. Maes, Phys. Rev. A **96**, 023864 (2017).
[24] D. E. Pelinovsky, D. A. Zezyulin, and V. V. Konotop, J. Phys. A: Math. Theor. **47**, 085204 (2014).
[25] A. Regensburger, C. Bersch, M. A. Miri, G. Onishchukov, D. N. Christodoulides, and U. Peschel, Nature (London) **488**, 167 (2012).
[26] H. Ramezani, T. Kottos, R. El-Ganainy, and D. N. Christodoulides, Phys. Rev. A **82**, 043803 (2010).
[27] E. Lazo and E. Diez, Phys. Lett. A **374**, 3538 (2010).
[28] E. Lazo and E. Diez, Phys. Lett. A **375**, 2122 (2011).
[29] E. Lazo, F. Mellado, and E. Saavedra, Phys. Lett. A **376**, 3423 (2012).
[30] E. Lazo and E. Diez, Physica B: Condens. Matter **419**, 19 (2013).
[31] E. Lazo, Physica B: Condens. Matter **432**, 121 (2014).
[32] E. Lazo, F. R. Humire, and E. Saavedra, Physica B: Condens. Matter **452**, 74 (2014).
[33] E. Lazo, C. E. Castro, and F. Cortés-Cortés, Phys. Lett. A **380**, 3284 (2016).
[34] E. Lazo, Eur. Phys. J. D **71**, 145 (2017).
[35] E. Lazo, F. R. Humire, and E. Saavedra, Int. J. Mod. Phys. C **25**, 1450023 (2014).
[36] E. Lazo, E. Saavedra, F. Humire, C. Castro, and F. Cortés-Cortés, Eur. Phys. J. B **88**, 2 (2015).
[37] E. Lazo, A. Garrido, and F. Neira, Eur. Phys. J. B **89**, 249 (2016).
[38] E. Lazo and F. Cortés-Cortés, Eur. Phys. J. Plus **134**, 28 (2019).
[39] E. Diez, F. Izrailev, A. Krokhin, and A. Rodriguez, Phys. Rev. B **78**, 035118 (2008).
[40] F. B. Pelap, J. H. Kamga, S. B. Yamgoue, S. M. Ngounou, and J. E. Ndecfo, Phys. Rev. E **91**, 022925 (2015).
[41] Y. J. Zhang, H. Kwon, M.-A. Miri, E. Kallos, H. Cano-Garcia, M. S. Tong, and A. Alu, Phys. Rev. Appl. **11**, 044049 (2019).
[42] M. Chitsazi, H. Li, F. M. Ellis, and T. Kottos, Phys. Rev. Lett. **119**, 093901 (2017).
[43] C. M. Bender, M. Gianfreda, and S. P. Klevansky, Phys. Rev. A **90**, 022114 (2014).
[44] S. V. Suchkov, B. A. Malomed, S. V. Dmitriev, and Y. S. Kivshar, Phys. Rev. E **84**, 046609 (2011).